Manuscript submitted to IET El.Pow.Appl.

MACC Modelling of Transformer Core Induction – Resolution and Accuracy

G. Shilyashki and H. Pfützner

Institute EMCE – Vienna Magnetics Group, TU Wien, Gusshausstr.27, 1040 Vienna, Austria

shilyashki@tuwien.ac.at

Abstract: As a tool for the optimization of transformer cores, numerical modelling is used to estimate local induction distributions. Compared to FEM, the Magnetic Circuit Modelling (MACC) uses much lower amounts of elements which raises questions of resolution and accuracy. This paper compares MACC-models of different resolutions, two flux paths (2FP) and four paths (4FP). Both are characterized by low computing times. The low resolution of 2FP offers compact information about global flux distributions, as a function of modified core geometry or material. The increased resolution of 4FP favours the assessment of regional concentration of rotational and circular magnetization. Comparisons with FEM illustrate that the latter is unsuitable for the identification of such mechanisms, if not complemented by post-processing. With respect to the over-all accuracy, the latter does not depend on the number of elements but on the accuracy of geometrical assumptions and allocated permeability functions. For the transverse direction and overlap regions, the corresponding accuracy values may be close to 10%, due to product tolerance or mechanical stress. Both high meshing densities and low approximation values (< 1%) are of academic nature. The attractiveness of modelling is not given by accuracy, but by revealing complex distributions with good approximation of instantaneous data.

1. Introduction

It is well known that even low variations of local induction values B in transformer cores prove to have a significant impact on local core losses P and on regional magnetostriction values λ, due to non-linear dependencies $P(B)$ and $\lambda(B)$. Therefore, evaluations of local induction values are highly relevant for the industry, with respect to optimizations of transformer cores. However, measurements of local induction values B may deviate from real values due to the need of specific core preparations - e.g. drilling holes for search coil wires, inter-lamina air gaps etc. The latter tend to influence flux distribution in specific ways. Furthermore, experimental measurements tend to be highly laborious and time consuming.

Due to the mentioned reasons, many authors use numerical methods, such as finite element method (FEM), for the estimations of B [1-5]. In the last 20 years, FEM has become the leading method for the assessment of magnetic quantities, such as local flux

distribution, eddy currents losses etc., of laminated cores of transformers, but also of rotating machines. As an advantage, FEM offers very high geometrical resolution. However, a well known disadvantage of FEM are high computational times. Furthermore, a restricted flexibility is given with respect to changed geometrical parameters of geometry.

Quite recently, we developed the novel multi-directional non-linear MACC-methodology (magnetic circuit calculation) [6-9], as a complement to FEM in cases of high complexity, but also for improved visualization of tendencies. Significant advantage of the methodology are (i) effective consideration of non-linear overlap characteristics in corners and T-joints, (ii) significantly lower computing time, (iii) possibilities of simple comparisons of modified core geometry, and (iv) presentations of results that favour technical and physical interpretations.

Compared to FEM, MACC uses much lower amounts of elements which raises questions of resolution and accuracy. The main aim of the here reported study was to investigate the impact of the number of elements on all three the computational time, the geometrical resolution and the accuracy of the investigate method. As a further aim, comparisons with FEM should be presented and discussed.

With respect to resolution, MACC modelling is discussed for the case of just two main flux paths (2FP) and that of four flux paths (4FP). For comparison, FEM modelling is presented that shows high resolution, as being typical for the method.

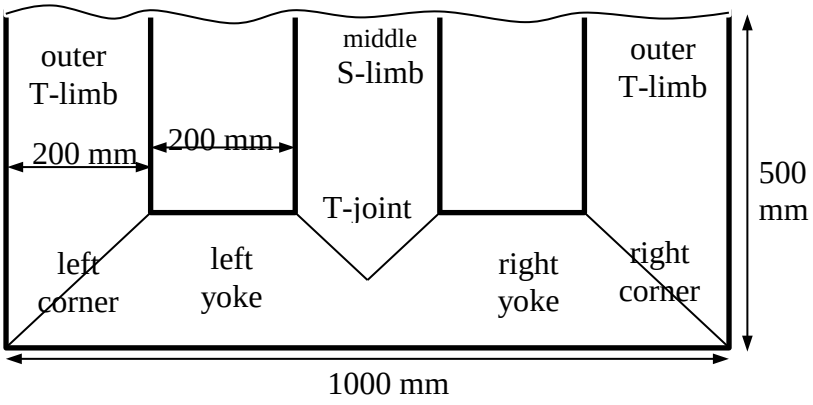

Fig.1. The modelled lower half of the investigated 3-phase, 3-limb transformer core package.

2. MACC-modelling

As described firstly in [6], MACC represents a specific procedure to apply equivalent circuit modelling for soft magnetic circuits, taking into account multi-directional non-linearities of the investigated material. MACC is a kind of a harmonization method which however should not be changed by mistake with other "harmonization methods" for transformer optimization such as [10]. The basic idea is to vary all local induction values until they agree with all the correspondingly adapted local permeability values, including the non-linear overlap reluctances. In the current paper, calculation of the flux distribution

by means of MACC-modelling is presented for a 3-phase, 3-limb transformer core package (Fig.1). We assume that it is stacked from highly grain oriented (HGO) material 27-ZDKH 95 with the following core dimensions: height and width 1000 mm, lamination width 200 mm and stacking height 20 mm. Furthermore, a multi-step-lap construction of overlaps is assumed and considered by the modelling.

For a 2D simulation, the relative permeability values μ_{RD} for magnetization in rolling direction (RD) and μ_{TD} in transverse direction (TD), as well as the impact of the overlap reluctances are needed, as input parameters. The corresponding data for the above given type of grain oriented material is presented in Fig.2. The permeability functions $\mu_{RD}(B_{RD})$ for RD and $\mu_{TD}(B_{TD})$ for TD, respectively, were obtained from a data catalogue [11]. Both functions show strongly non-linear behaviour, with maximal values close to B_{RD} = 0.8 T and B_{TD} = 0.9 T, respectively.

The behaviour of overlap regions in corners and T-joints is modelled by the assumption that flux flows in diagonal direction (DD), averaging over lamination pairs with RDs perpendicular to each other. Due to the fact that a length of overlap region cannot be defined, the permeability function is replaced by the corresponding overlap reluctance function $R_{DD}(B_{DD})$. The functions as given in Fig.2c were roughly estimated from data in [12]. Also this function shows a pronounced non-linearity. Starting at the so-called critical induction close to 1.3 T, it exhibits a steep slope. In Fig.2c, R_{DD} is given for an overlap region of a diagonal width w_{DD} = 100 mm · 1.41 for 2FP and for 50 mm ·1.41 for 4FP.

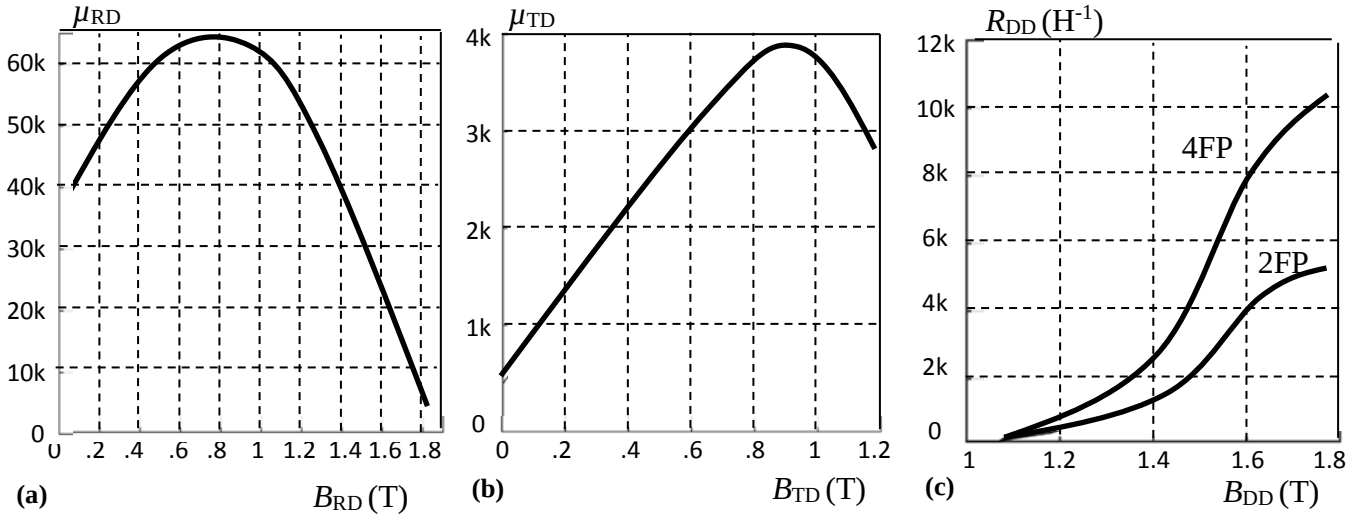

Fig.2. Data of the investigated electrical steel 23ZDKH95. (a) Relative permeability μ_{RD} in rolling direction, as a function of the induction B_{RD} [11]. (b) μ_{TD} in transverse direction, as a function of B_{TD} [11]. (c) Overlap reluctances R_{DD} as a function of the induction B_{DD} for two-path modelling and four-path modelling, respectively (roughly estimated from [12]).

According to many publications, both losses and magnetostriction tend to rise significantly with increasing flux distortion due to circulating magnetization (CM) and due to rotational magnetization (RM). The latter arises in T-joints and yokes round instants of zero-flux in an outer limb, i.e. R-limb or T-limb, as MACC-modelled in [7,8]. On the other hand, RM in the end of the middle S-limb arises round the instant of zero-flux in the middle S-limb. For the first time, this instant is specifically modelled here, for a

nominal induction B_{NOM} = 1.7 T. This means that the middle limb shows a global induction B_S = 0. The global induction of the R-limb B_R = 1.7 T · cos 30° = 1.47 T is taken over by the T-limb, according to B_T = - 1.47 T (Fig.3).

3. Modelling with minimum resolution

For a specific discussion on resolution and accuracy of the modelling, this paper compares two models of different resolutions – i.e. two main flux paths (2FP) and four main paths (4FP), respectively. The case of minimum resolution is restricted to a window path and a peripheral path, according to Fig.3. Each of them is represented by a series of magnetic reluctances R_{RD} and R_{DD}, in RD and DD, respectively. The interactions between the two paths is considered by reluctances R_{TD} in TD. The resolution in the regions with - as expected - more complex flux distributions like T-joint and corners is increased, considering shorter flux path elements in those areas. As a whole, the 2FP model consists of 58 flux path elements, 37 in RD, 15 in TD and 6 in DD.

Fig.3. presents results of instantaneous modelling for the above defined instant. It includes local induction values B_{RD}, B_{TD} and B_{DD}. Also the corresponding permeability values μ_{RD} and μ_{TD} are given to characterize the instantaneous behaviour of material at the given location. Finally, the corresponding instantaneous reluctance values R_{RD}, R_{TD} and R_{DD} are given to compare local differences of needed excitation. However, for quantitatively exact comparisons of values of R_{DD}, possible differences of the corresponding element volumes have to be considered. The compact multi-parametric data presentation according to Fig.3 offers a significant advantage of the novel MACC-methodology, as demonstrated by the following.

Fig.3. shows that the global flux in the R-limb is split into two portions. While the portion of the outer flux path “flows” towards the T-limb without any obstacles along the periphery, the inner path crosses the T-joint region. In spite of the latter, and also in spite of different path lengths, the two flux portions are very similar to each other. As an explanation, the overlap regions of corners represent high instantaneous reluctance values R_{DD} exceeding 1.5 kA/Vs. This is equivalent to more than 100 mm long sections of yoke material magnetized in RD, thus yielding a strongly balancing function. Interesting enough, the limb shows a weak inner flux concentration, while the yoke shows an outer one, mediated through flux in TD.

The V-end of the S-limb represents a significant impediment, due to extremely high anisotropy of the investigated HGO-material, according to low μ_{DD}. Thus, in the T-joint, a significant part of the flux (with B_{RD} = 1.38 T) enters the S-limb through a sharp turn. Entered in the middle limb, the flux is divided into two portions. The first one continues its way along the RD of the middle limb, significantly supported from the very high permeability values B_{RD} up to 60 000. With 1.13 T, a high portion of about 75% of flux passes over to the upper core half in the course of circulating magnetization round the left window. As it is well known, this circulating magnetization causes significant distortion of the waveform of the flux, corresponding to higher harmonics. This yields increased eddy current losses, as well as higher harmonics of magnetostriction.

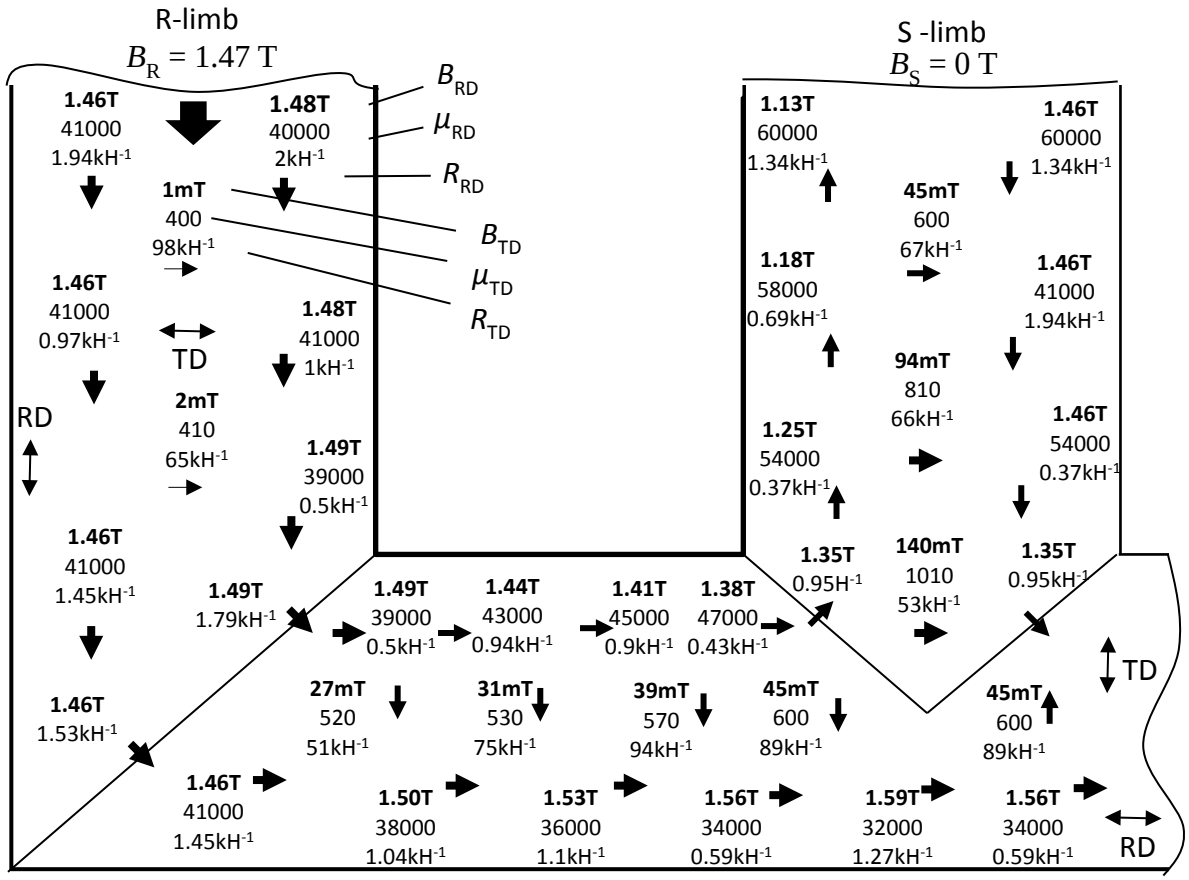

Fig.3. Local flux distribution for the time instant of zero flux in the middle S-limb. Local induction values in RD and DD are in T, those in TD in mT. Below: local instantanious permeabilities μ_{RD} and μ_{TD}, as well as the resulting instantaneous reluctance values in kH^{-1} in RD, TD and DD.

The other, significantly lower portion (B_{TD} = 140 mT), leaves the middle limb, continuing its way towards the T-limb, supported by the relative high value of the permeability in TD close to μ_{TD} = 1000, strengthened by the non-linearity of the function $\mu_{TD}(B_{TD})$ (compare Fig.2b). The second portion arises in the course of rotational magnetization (RM) of an axis ratio $a = B_{TD}/B_{NOM} \approx 0.1$. As already mentioned, RM causes distinct regional increases of both losses and magnetostriction. Here it should be mentioned that the instantaneous flux distributions of Fig.3 are in good principal agreement with experimental results from thin foil sensors that were arranged interlaminarely in the interior of a model core of similar type of highly grain oriented material.

Summarizing, in spite of minimum resolution, MACC-modelling with two main flux paths (2FP) proves to be entirely sufficient for gaining a global overview of flux distributions. For example, consequences of widened windows can easily be predicted by corresponding adjustments of yoke elements (elongation of RD-elements and broadening of TD-elements). Important quantitative analyses - e.g. for the strength of rotational and/or circulating magnetization - can be performed in simple ways. However, for more

detailed *local* analyses - for example about the strength of harmonics - a finer resolution with more flux paths may be preferable. This is discussed in the next section.

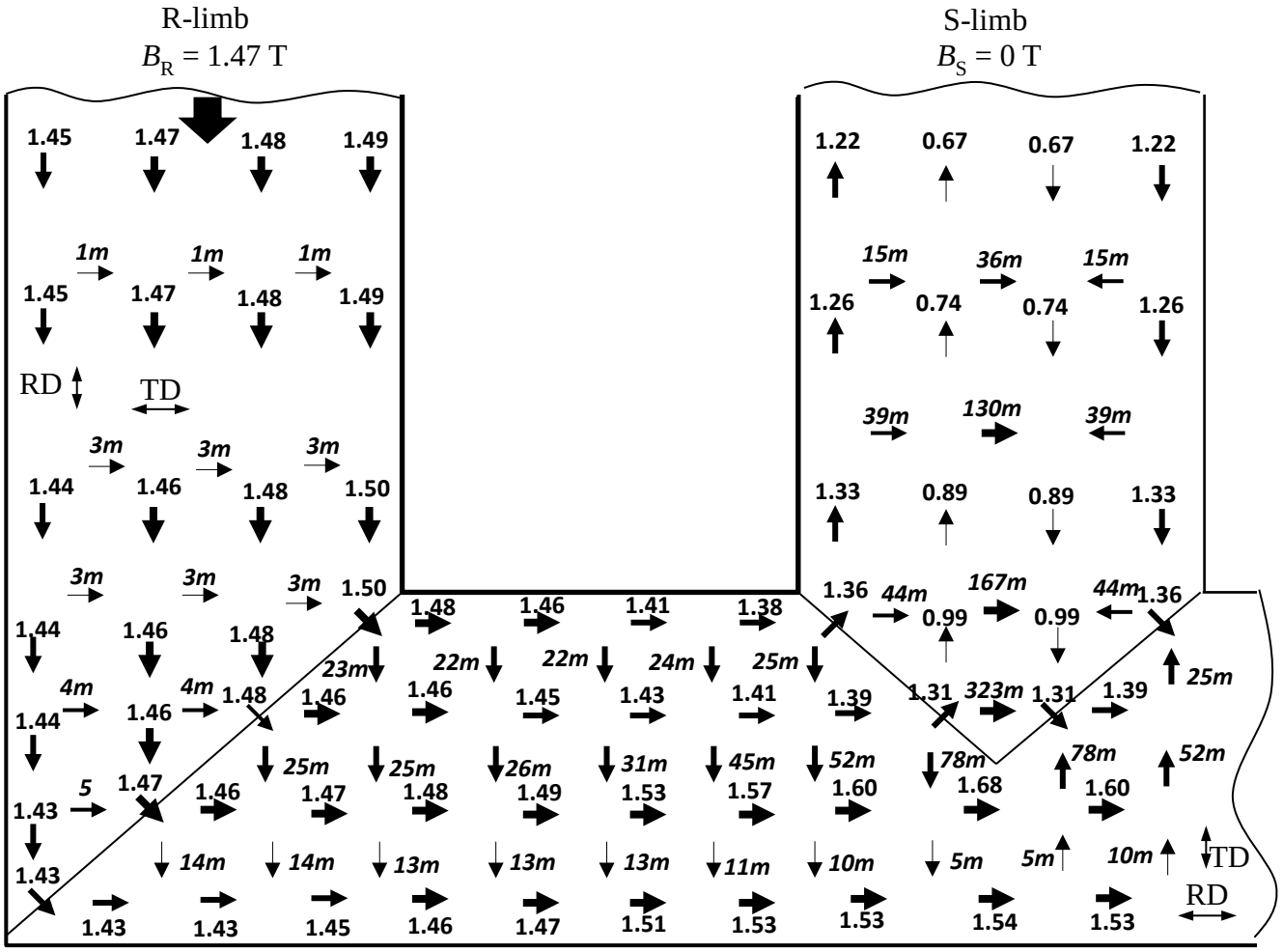

Fig.4. Local instantaneous distribution of induction values B_{RD}, B_{TD} and B_{DD}, for the time instant of zero flux in the middle S-limb, assuming four main flux paths (4FP). All induction values B_{RD} and B_{DD} are given in T, values B_{TD} in mT.

4. Modelling with increased spatial resolution

Aiming for increased spatial resolution, the results of induction distributions of Fig.4 are based on four main paths of flux (4FP). Compared to 2FP with 58 flux path elements, the present model considers much more elements, the total number being 188. We assumed 102 volume elements in RD, 74 in TD and 12 in DD. This means that the resolution is more than doubled.

As an advantage, the image reveals differences between middle and peripheral locations of the different core regions. No win is attained for the R-limb which reveals a continuous, weak increase of B_{RD} towards the window. In the yoke, we see an unexpected, weak maximum in the 3rd row of elements. However, these details can be assumed to lack practical relevance.

Increased relevance is given for mechanisms that influence losses or magnetostriction in non-linear ways. The S-limb shows a strong concentration of flux at the peripheries which means that eddy current losses can be assumed to be intensively enhanced here. As well, with B_{TD} = 323 mT, the graph indicates a distinct concentration of rotational magnetization at the lower part of the V-element of S-limb. As a conclusion, we can expect regional maxima of both losses and magnetostriction, which however are influenced also by flux distributions at other instants (in particular, in instants of zero-flux in outer limbs; see [7]).

We summarize that the improved resolution helps for conclusions on non-linear behaviours. On the other hand, we assume that 2FP presentations offer much clearer insights to the *global* distributions of flux. The latter prove to be mantled by the high amount of data of the 4FP-case.

Of course the higher number of elements for 4FP yields increased computation times. For example, in the here given case it was less than 1 s. In practice, these differences are insignificant, even if dynamic modelling is applied (e.g. for 90 instants of the period, taking advantage of symmetries). As reported in [7], the corresponding times are of the order of 1.5 minutes (1 s for a time instant). As an example, Fig.5 shows dynamic RM patterns, as resulting for rotations of the induction vector $\boldsymbol{B}$ for 2FP and 4FP, respectively. Also the latter results were attained in rapid ways, within minutes, as a general advantage of MACC-modelling.

As well known, higher computing times are typical for FEM, due to the need of high numbers of elements, and also due to complicated mathematics in the course of energy minimization. For comparison, we modelled the here studied core by means of the commercial FEM software COMSOL. Fig.6 shows a corresponding result, assuming 5327 elements, according to strongly increased resolution. The computing time was close to 4 s, i.e. not much higher than for MACC - however, due to a significant neglect as discussed further down. Local intensities of induction are coded by both the spacing of flux lines and by shading. In spite of high resolution, it is questionable if the results offer corresponding improvements of interpretation. For example, it is difficult to identify tendencies of distributions of transverse flux, in particular with respect to rotational magnetization. In principle, it would be possible also here to determine global portions of flux, but this would need specific post-processing.

It should be mentioned that the FEM-image of Fig.6 does not consider the impact of overlaps in corners and T-joints. We tried to perform an approximate consideration by definition of extra-regions of increased meshing density. This procedure yielded computing times of the order of 13 seconds, compared to less than 1 s for MACC.

However, as a main disadvantage, approximation could not be reached at all for certain instants of time. On the other hand, the neglect of overlap impact - as in the case of Fig.6 - would represent a systematic source of error, as discussed in the following section.

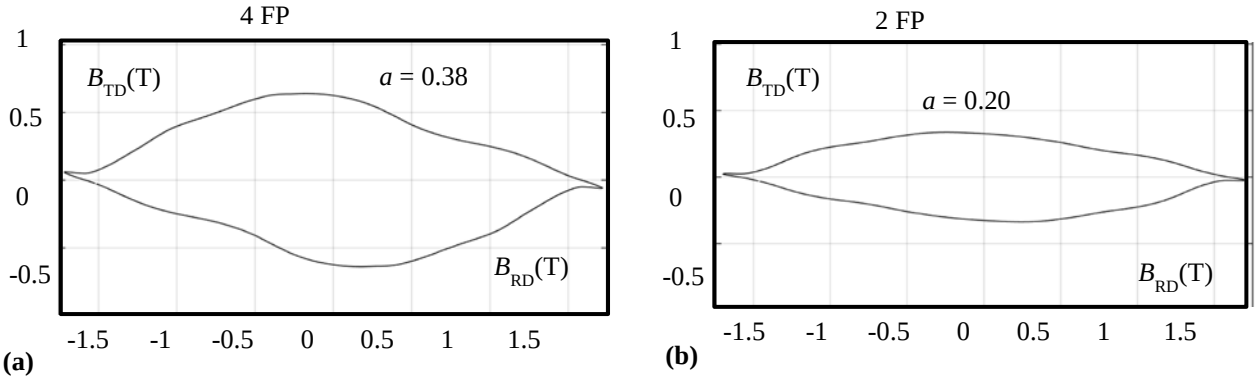

Fig.5. Vector magnetization patterns $\boldsymbol{B}(t)$ for the T-joint region below the V-end at the side of the yoke. This is the location with the strongest rotational magnetization.
(a) 4FP-modelling, yielding an almost doubled axis ratio a. (b) 2FP-modelling.

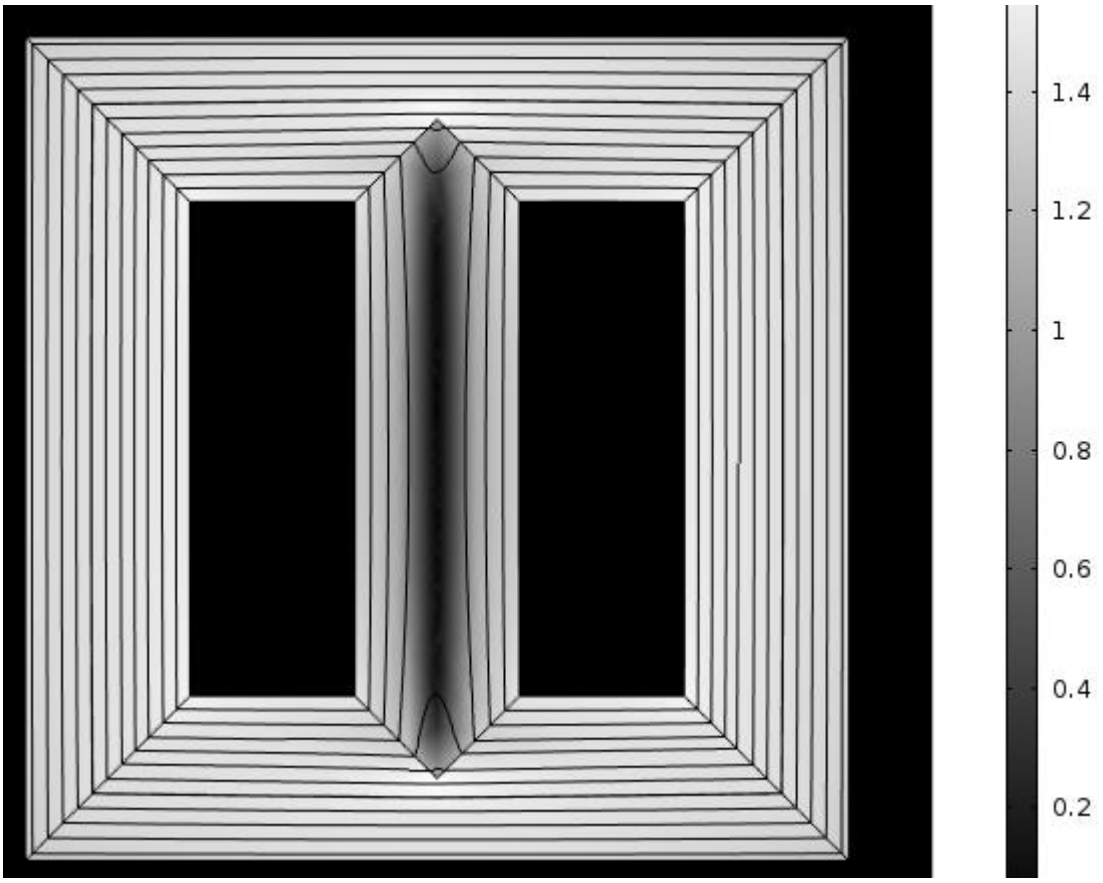

Fig.6. Comparison result as attained from FEM modelling of high resolution, however neglecting effects of overlap regions in corners and T-joints. Differences of local induction are coded by colour. *Notice:* Rotational magnetization is indicated also here, i.e. through bowed arrows at T-limb ends.

6. Aspects of accuracy

With two or four main flux paths according to Fig.3 and Fig.4, respectively, very low spatial resolution is given. In principle, the resolution can be increased with support from a meshing generator. However, this would reduce the attractiveness of MACC, the latter being given by effective indications of tendencies of regional flux distributions.

In principle, also the *directional* resolution can be increased, by consideration of further values of the angle ψ between the RD (according to $\psi = 0$) and the TD ($\psi = 90°$). It suggests itself to consider $\psi = 45°$, but this remains without profit since this direction is close to the so-called hard direction $\psi = 55°$. As a matter of fact, the here discussed version of MACC is specifically adapted to Goss texture where magnetization processes are mediated through re-distributions of atomic magnetic moments between the crystalline directions [001] (represented by the RD) and [010]*[100] (represented by the TD). Weak magnetizations in other angles ψ result as vector sums of magnetization steps in RD and TD.

An exception is made for overlaps of joints where the diagonal direction DD is introduced. It considers that the RDs of two neighboring laminations are perpendicular to each other which means that a global magnetization in DD represents the mean of two flux components in RD. By the way, our experience shows that the introduction of DD-elements into FEM (COMSOL) is possible with restrictions, however, causing distinct increases of computing time. On the other hand, tests indicate that lacking consideration of the DD may yield distinct errors throughout the core in the order of about 10%. The reason is given by the steep slope of the function $R_{DD}(B_{DD})$ for $B_{DD} > 1.3$ T , according to Fig.2c.

With respect to accuracy, a main problem is given by an effective definition of the latter term. In the given case of modelling, a local numerical result of MACC concerns an instantaneous value out of the induction time functions $B_{RD}(t)$, $B_{TD}(t)$ or $B_{DD}(t)$ that would arise in a physical core that is assumed as the basis of the modelling. This means that the error expresses the percentage deviation $e = 100\ (B_M - B_R) / B_R$ of the value B_M estimated from modelling and that B_R of the real, physical core.

Table 1 Levels of numerical modelling procedure

level L7 - post-processing (data presentation)
level L6 - process of approximation
level L5 – assumption of approximation start values
level L4 - definition of border conditions
level L3 - allocation of material characteristics
level L2 - design of network (definition of elements)
level L1 - establishment of geometrical model

Considering the procedure of MACC modelling as described in Section 2, contributions to the error e can be expected on seven levels as defined in Table 1. In principle, these levels are valid for all numerical methodologies, including FEM. The here used 2D-MACC distinguishes elements for the three directions RD, TD and DD. They are error-prone in different ways. From experience, minimum deviations arise for the RD, much higher ones for the TD and the DD.

A significant source of systematic error results on level L1, i.e. the outline of geometrical details of the model. The above example of core was assumed to represent the largest main package of a transformer core, of maximum thickness. However, it is well known that the individual core packages are in interaction through off-plane fluxes (e.g. [13]). Restricting modelling to 2-dimensional meshing means that significant errors (as deviations of “real” distributions of induction B_R) are accepted a priori. For the total of package, they may be of the small order of 1%, as a very rough estimation. But -even for the RD - the deviation of *regional* values close to joints of corners and T-joints, may be of the order of several percent.

As it is well known, the corners of core windows exhibit “air triangle" regions, according to lowered effective lamination width. While their effects can be considered by MACC in effective ways [9], they were neglected in the here presented modelling. This neglect contributes to errors significantly. However, it saves computing time, in particular in the case of FEM. This is due to the large amount of elements, and also due to complicated mathematics in the course of energy minimization (involving time-consuming steps of differentiation and integration).

From experience, the most significant source of error is given on level L3, the allocation of material characteristics to the individual elements. Critical are DD-elements (see Fig.2c), e.g. regional variations of airgap lengths in joints, influencing global flux distributions. Even more relevant effects result from variations of TD-elements, due to the fact that they determine the distribution of rotational magnetization and circular magnetization, respectively. The first one has strong influence on losses and magnetostriction, the second one on flux distortions and thus on eddy current losses. Steel production tolerances - but also local mechanical stresses within the clamped core - may change the slope of the function $\mu_{TD}(B_{TD})$ (Fig.2b) in strong ways corresponding to errors up to the order of 20%.

The above strong sources of errors at the low levels (L2, L3) mean that those at high levels (L5, L6) can be seen as rather irrelevant. That is, for the total error at a given element - according to the further above defined error e -, "low" levels of approximation (e.g. of 1%) are insignificant. Vice-versa, long procession times in order to attain e.g. 0.1% are not justified due to the fact that they are of mere academic nature.

7. Main conclusions

The above described study concerns the numerical modelling of induction distribution of a transformer core package by MACC, assuming two main flux paths (2FP) and four paths (4FP), respectively. Comparisons were made with FEM (COMSOL). The main conclusions of the study are the following:

(1) Lowest resolution corresponding to 2FP reveals global flux distributions (peripheral side - window side) in effective ways, e.g. indicating consequences of modified core design, on rotational magnetization (RM) or circular magnetization (CM).

(2) Increased resolution (4FP) mantles global portions. But it reveals local differences of induction which is significant e.g. for the assessment of eddy current losses that rise in a non-linear way.

(3) Considering the short calculation time of 2-dimensional MACC suggests a coupling of 2FP and 4FP.

(4) FEM of a priori high resolution tends to yield graphic results that complicate

quantitative assessments of flux portions, if specific post processing is not performed.
(5) Both MACC and FEM allow for approximation below 1% which however does not define the true error of modelling.
(6) Most significant systematic errors (10%, or more) tend to result from difficulties to define the permeability function $\mu_{TD}(B_{TD})$ for magnetization in transverse direction.
(7) Strong systematic errors (up to 10%) may also result from erroneous consideration of overlap regions.
(8) With these potential errors, numerical modelling cannot be expected to yield exact quantitative results in a general way. Rather, the significance is given by simple and rapid estimations of general consequences of modified parameters of material and/or geometry, in the course of core optimization.

8. Acknowledgement

The authors thank for support of the Austrian Science Funds FWF (Project number P 28481-N30, "MagFoilSensors")

9. References:

1. J. Shazly, A.A. Adly, "Extensions to the Finite Element Technique for the magneto-thermal analysis of aged oil cooled-insulated power transformers", *J.Electrom.Anal.Appl.* 4, pp. 167-176, (2012).

2. M. Khelil, M. Elleuch, "Modeling of the air-gaps of overlapped joints in three-phase transformer iron core for using by FEM. *Proc. 6th Int. Conf. on Syst. Sig. Dev.*, pp.1-6 (2009).

3. R. Haettel, M. Kavasoglu, A. Daneryd, C. Ploetner, "Prediction of transformer core noise. Proc. COMSOL Conf. Cambridge, 1-6 (2014).

4. D.Constantin, P.M.Nicolae, C.M.Nitu,"3D finite element analysis of a 3-phase power transformer," IEEE Proc. EuroCon Zagreb, 1548-1552 (2013).

5. Q.Tang, S.Guo, Z.Wang, "Magnetic flux distribution in power transformer core with mitred joints." *J.Appl.Phys.* 117, 17D522, (2015).

6. H.Pfützner, "Procedure for the calculation of 3-dimensional induction distributions (in German)," Austrian Patent, pending, 2014

7. H.Pfützner, G.Shilyashki, G.Trenner, E.Gerstbauer,"Multi-directionally non-linear magnetic equivalence circuit calculation (MACC) of rotational magnetization intensity in transformer cores", *IJAEM*, 2016, **50**, pp. 81-95

8. G. Shilyashki, H. Pfützner, P. Hamberger, M. Aigner, E. Gerstbauer, M. Palkovits, G. Trenner, "Numerical prediction of rhombic rotational magnetization patterns in a 3-phase transformer core package", *IEEE Trans. Magn.*, 2016, **52**, (1), 7200110

9. G. Shilyashki, H. Pfützner, E. Gerstbauer, G. Trenner, P. Hamberger, M. Aigner, "Inhomogeneity and local distortions of magnetic flux in a single phase transformer core package," *IEEE Trans.Magn.* **52**-11, 7210109 (2016).

10. H.V.H. Ayalla, D.S.Coelho, V.C.Mariani, M.V.F.Luz, J.V.Leite, “Harmony search approach based on ricker map for multi-objective transformer design optimization” IEEE Trans.Magn.51, ID 7202304 (2015).

11. Nippon Steel Corporation Catalogue, EXE 320: “Technical Data an Orientcore-HI-B“

12. Nussbaum, C., Pfützner, H., Both, T., Baumgartinger, N., Ilo, A., Clabian, M. "Neural Networks for prediction of transformer core characteristics", *IEEE Trans. Magn.*, 2000, **36,** pp. 4523-4533

13. G. Shilyashki, H. Pfützner, P. Hamberger, M. Aigner, F. Hofbauer, I. Matkovic, A. Kenov, “The impact of off-plane flux on losses and magnetostriction of transformer core steel,” *IEEE Trans. Magn.* 50-11, 8401604 (2014).